3

Material Issues in AMOLED

Jong Hyuk Lee, Chang Ho Lee and Sung Chul Kim
Samsung Mobile Display, San #24 Nongseo-Dong, Giheung-Gu, Yongin-City, Gyunggi-Do, Korea 446-711

1. Introduction

Since the first mass production of AMOLED (active matrix organic light emitting diode) for mobile display in 2007, many companies have dived into the market for mobile phones and the other potable displays based on extraordinary image qualities of AMOLED. In a mass production point of view, small-sized AMOLED almost attained a stage of technological maturity. However, it still needs some more improvements in terms of materials for lower power consumption, longer life time of AMOLED. Besides outstanding market expansion of AMOLED in mobile applications, AMOLED also can bring us new displays that are only shown in some SF movies, such as paper-thin, foldable, bendable and transparent displays.
In terms of power consumption, AMOLED is intrinsically superior to LCD, where the backlight should be always "on". If we consider that the on-ratio is usually less than 30% in most TV broadcastings, a big advantage exists for AMOLED because AMOLED turn on the light for each pixel individually. Moreover, AMOLED still have plenty of rooms to further reduce power consumption. Although low power consumption is the reason why AMOLED is a better choice for portable devices, recent trend of green business require consuming lower power for brighter display. In order to meet those stringent requirements, new materials with high efficiency and optimization of AMOLED device structure is necessary.
This article reviews current material issues of AMOLED for general application and for unique application such as transparent and bendable displays.

2. Organic material issues of amoled

2.1 Materials for hole transporting

Since the first report of multi-layered OLEDs, many studies have focused on improving device efficiency and enhancing the durability of OLEDs. Development of new materials for improving device performance such as device driving voltage, efficiency, and life-time is one of the major research subjects in the OLED research area. And there have been lots of progress in performance characteristics. Despite much improved device performance, an insufficient life-time remains one of the primary issues limiting the wide-spread commercial use of OLED. Life-time property is a major obstacle in the competing with liquid crystal display (LCD) as flat panel displays and, life-time related image sticking is an emerging issue of OLED operation.

For the fabrication of highly stable OLEDs, specific optical and electronic properties, such as fluorescence, energy levels, charge mobility etc, and high morphologic stability are required [1-4]. The electrochemical stability of materials used in OLED is very important to improve the device properties. Also, the thermal stability of hole-transporting material is one of the significant factors of the device durability. Under thermal stress, most organic glass transition materials tend to turn into the thermodynamically stable crystalline state, which leads to device failure [5, 6]. It is known that an amorphous thin film with a high glass transition temperature (T_g) is more stable to heat damage [7-11]. In general, high thermal stability, especially high T_g above 100 °C, good hole transporting ability, and excellent film formability are essentially needed for the hole-transporting materials. Various triarylamine derivatives have been utilized as hole-transporting materials (HTMs) because of their good film forming capabilities as well as good hole-transporting abilities [3, 12-13].
The radical cation is one of important reactive intermediate in organic molecules and it can be obtained by loss of single electron from neutral molecules. The chemical structures of common radical cation species are shown in Fig. 1.

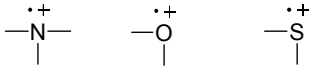

Fig. 1. The common radical cation species

Both hole and charge are not necessary to be localized together on one atom and they can be delocalized over the whole molecule. In fact, the delocalization of the unpaired electron in conjugated system can lead to stable radical cations such as the Wurster salt. This compound is isolable and the chemical structure including its resonance forms are shown in Scheme 1. Aryl amine moieties are thought to be a main core structure in HTMs because amine atom is relatively easy to lose one electron and the resulting radical cation can be stabilized by resonance effect of adjacent aryl substituent. It is worth to note that the Wurster salt mentioned above is stabilized by two factors. One is a resonance effect by aryl substituents and the other is stabilized by counter ion, perchlorate.

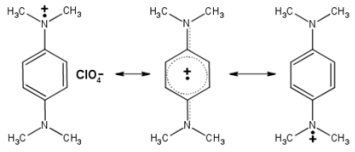

Scheme 1. The possible resonance forms of Wurster salt

However, there is no such stabilization by counter anion in OLED devices. The stability of radical cation mainly depends on its adjacent substituent. Therefore the HTMs stabilized by their substituents are one of important factors to improve the OLED performance.
There are several factors contributing to the stability of radicals. Those are hyperconjugation, resonance, hybridization, captodative effect, and steric effect [24]. Among them resonance and steric effect are important in aryl aminyl radical cations. These aminyl radical cations can be reactive and there are many possible reactions such as fragmentation, dimerization,

disproportionation, and, oxidation. However, the first three reactions are not favorable in OLED device because these give rise to change of the original HTMs via formation or cleavage of σ bond. It is thought to be one of plausible reasons for OLED degradation. However, the oxidation is desirable in OLED device because this single electron transfer process between adjacent molecules results in a hole-transporting process, a fundamental reaction of HTMs. Fragmentation and disproportionation reaction is relatively less important in solid state because the interactions between each radical cations are small but the interactions between a molecule and solvent are strong in solution. In contrast, the dimerization and the oxidation reaction are more important in solid state owing to their strong interaction between radical cation each other. The following Scheme 2 summarizes the important reactions in OLED device.

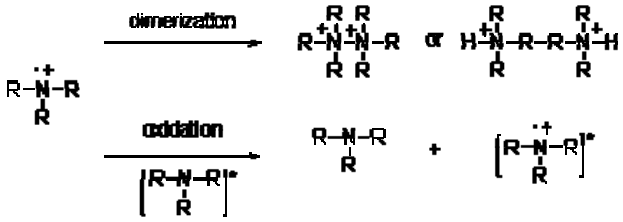

Scheme 2. Dimerization vs oxidation reaction

Therefore HTMs have to be modified to increase the stability of aminyl radical cation which can result in minimizing the cleavage of σ bond in molecules. Furthermore resonance effect and steric factor have to be considered to minimize the dimerization reaction in solid state.
Recently, considerable efforts have been devoted to the development of new amorphous triarylamines possessing high morphologic stability [14-20]. We have already reported that the device employing thermally stable hole-transporting materials showed high efficiencies [21, 22]. However, it is thought that these hole-tansporting materials cannot meet high efficiency and long lifetime simultaneously. Therefore, we will discuss how to modify the structure of HTMs in order to increase their radical cationic stabilities. In addition, device performance with these modified molecules will be discussed.

2.1.1 Physical properties of hole transporting materials

Tested molecules having hole-transporting properties are shown in Fig. 2.

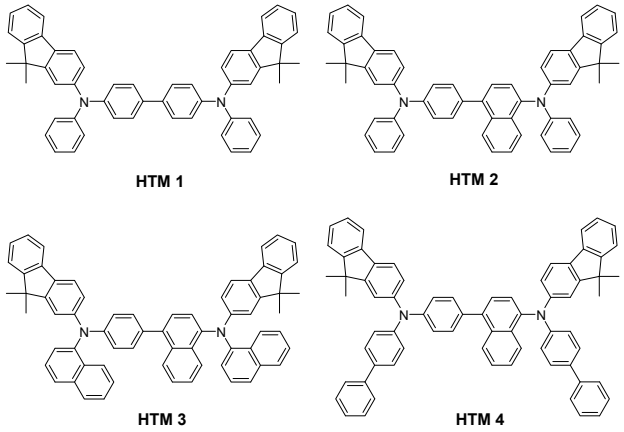

Fig. 2. Hole-transporting materials

Absorption spectra were measured with a HITACHI U-3000 UV spectrophotometer. ^{1}H NMR and ^{13}C NMR spectra were recorded with a JEOL JNM-ECP 400 FT NMR spectrometer. Differential scanning calorimetry (DSC) was performed on a TA Instruments, DSC-2910 unit using a heating rate of 10 °C/min and a cooling rate of 40 °C/min. Samples were scanned from 30 to 300 °C, cooled to 0 °C, and then scanned again from 30 to 300 °C. The glass transition temperatures (T_g) were determined from the second heating scan. Thermogravimetric analysis (TGA) was undertaken on a TA instrument, TGA-2050. The thermal stability of phenylnaphthyldiamine derivatives was determined under a nitrogen atmosphere, by measuring weight loss while heating at a rate of 20 °C/min. The results are summarized in Table 1 along with literature data of common hole-transporting materials for comparison. The ionization potentials (IPs) of materials used in device fabrication were determined by ultraviolet photoelectron spectroscopy (UPS) (Riken Keiki, AC-2) using the samples prepared by PMMA polymer binder on glass and the energy levels of lowest unoccupied orbital (LUMO) were approximately defined as differences between IPs and long wavelength cutoffs of the absorption spectra of 0.2 mM CH_2Cl_2 solution.

As mentioned before, a radical cation of **HTM 2** is more stable than that of **HTM 1** by two factors. As shown in structure A and B, the naphthyl amine radical cation B is preferred because it has two more resonance forms than cation A. It is well known that molecules having more resonace form are more stable. In addition, cation B can be stabilized further by steric effect. A bulky naphthyl moiety which is bigger than phenyl moiety can retard dimerization of radical cations.

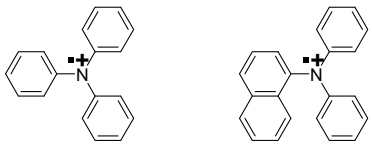

A B

The thermal stability data of these three phenylnaphthyldiamine derivatives, **HTM 2-4**, were investigated by differential scanning calorimetry and thermogravimetric analysis; the

results are summarized in Table 1 with the well-known hole-transporting material **HTM 1** for comparison. As shown in Table 1, all three phenylnaphthyldiamine-cored HTMs (**HTM 2-4**) have higher value of T_g relative to their biphenyldiamine analog **HTM 1**, proofing the high morphologic stability of the amorphous phase in a deposited film, which is a prerequisite for the application in organic electroluminescent devices.
According to Shirota [1], a non-planar molecular structure preventing easy packing of molecules and an increased number of conformers in the molecule are preconditions in the design and synthesis of amorphous molecular glasses. Glass formation is enhanced by incorporation of bulky substituents. The incorporation of bulky substituents also hinders translational, rotational and vibrational motions of molecules, leading to an increase in the T_g. We attribute to the increase in the morphological stability of the biphenyl-based material to the presence of naphthalene substituents at the central phenylnaphthyl core, which may hinder the crystallization process. It is important that OLEDs be constructed from materials having a relatively high value of T_g to avoid problems associated with crystallization, which leads to device degradation.
The HOMO and LUMO levels of these phenylnaphthyldiamine derivatives are also listed in Table 1. The HOMO was determined using a photoelectron spectrometer, while LUMO was calculated based on the HOMO energy level and the lowest energy absorption edge of the UV absorption spectrum. The HOMO and LUMO levels of these compounds were measured at ca. 5.40 - 5.45 eV and 2.43 - 2.53eV, respectively.

Compounds	T_d[a] (°C)	T_g[b] (°C)	T_m[b] (°C)	T_c[b] (°C)	λ_{max}[c] (nm)	HOMO[d] (eV)	LUMO[e](eV)
HTM 1	380	121	264	NA	360	5.40	2.38
HTM 2	395	159	296	NA	342	5.40	2.43
HTM 3	430	167	225	NA	355	5.45	2.53
HTM 4	423	174	255	NA	353	5.45	2.48

[a] Obtained from TGA measurement. [b] Obtained from DSC measurement. [c] Measured in CH_2Cl_2 solution. [d] Determined by ultraviolet photoelectron spectroscopy (UPS). [e] Calculated based on the HOMO level and the lowest energy absorption edge of the UV spectrum.

Table 1. Physical properties of the phenylnaphthyldiamine derivatives and biphenyldiamine derivative **HTM 1**

2.1.2 Device fabrication and characteristics

Prior to device fabrication, ITO with a resistance of 15 Ω/□ on glass was patterned as an active area of 4mm² (2mm x 2 mm) square. The substrates were cleaned by sonication in deionized water, boiled in isopropylalcohol for 20 min, and dried with nitrogen. Finally, the substrates were treated with UV/ozone for 20 min. Organic layers were deposited sequentially by thermal evaporation from resistively heated alumina crucibles onto the substrate at a rate of 0.5 – 1.0 Å/sec in the organic chamber. The base pressure at room temperature was 3 x 10^{-6} Torr. The deposition rate was controlled using a ULVAC crystal monitor that was located near the substrate. After organic film deposition, the substrate was transferred to another chamber maintaining the base pressure of 3 x 10^{-6} Torr. Before the deposition of metal cathode, LiF was deposited onto the organic layers with the thickness of

10 Å. A high-purity aluminum cathode was deposited at a rate of 4–8 Å/sec with the thickness of 3000 Å as the top layer. After the metal chamber was vented with N_2 gas, the device was immediately transferred to an N_2-filled glove-box upon fabrication. A thin bead of epoxy adhesive was applied from a syringe around the edge of a clean cover glass. To complete the package, a clean cover glass was placed on the top of the device. The epoxy resin was cured under intense UV radiation for 5 min. The current–voltage characteristics of the encapsulated devices were measured on a programmable electrometer having current and voltage sources, Source Measure Unit, model 238, (Keithley). The luminance and EL spectra were measured with a PR650 system (Photo Research). The current–voltage, EL spectra and luminance measurements were carried out in air at room temperature. Only light emitting from the front face of the OLED was collected and used in subsequent efficiency calculations.

To evaluate hole-transporting ability of newly synthesized phenylnaphthyldiamine derivative **HTM 2**, we fabricated the hole-dominant device using **HTM 2** as a hole-transporting material with structures as follows: ITO/2-TNATA/**HTM 2**/EML/Al (device II). On ITO substrate, 4´,4´´-tris(*N*-(naphth-2-yl)-*N*-phenyl-amino)tri- phenylamine (2-TNATA) was previously deposited as a hole-injecting material. IDE 215 doped with 3 % of IDE 118 (host and dopant materials by Idemitsu Co., LTD) was used as blue emitting layer.

		Al (3000 Å)	Al (3000 Å)
		EIL (10 Å)	EIL (10 Å)
Al (1500 Å)	Al (1500 Å)	ETL (250 Å)	ETL (250 Å)
EML (300 Å)	EML (300 Å)	EML (300 Å)	EML (300 Å)
HTM 1 (500 Å)	**HTM 2** (500 Å)	**HTM 1** (300 Å)	**HTM 2-4** (300 Å)
HIL (500 Å)	HIL (500 Å)	HIL (600 Å)	HIL (600 Å)
ITO	ITO	ITO	ITO
Device I	**Device II**	**Device III**	**Device IV-VI**

Fig. 4. Structures of EL devices used in this study

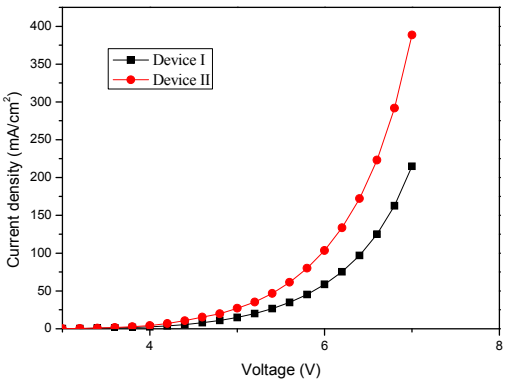

Fig. 5. Current density-applied voltage characteristics of device I and II

A reference device I composed of **HTM 1** as a hole-transporting material with the same thickness was also constructed for comparison (Fig. 4). The current-voltage (I-V) characteristics of the devices are shown in Fig. 5. The current density of the device II prepared with **HTL 2** is almost twice higher than that of the reference device I (103.4 mA/cm^2 vs 58.5 mA/cm^2 at 6 V). These outcomes showed that the hole-transporting ability of a phenylnaphthyldamine-cored **HTM 2** was highly improved than that of biphenyldamine-cored **HTL 1** due to its more resonance form in the radical cation as well as the steric effect of a naphthyl moiety resulting in efficient carrier transportation.

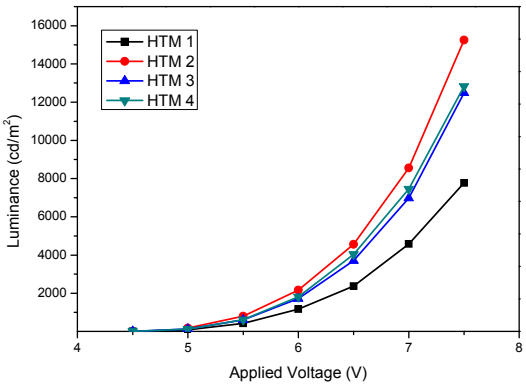

Fig. 6. Luminance-applied voltage characteristics of devices III-VI.

We also expected the stability of the phenylnaphthyl core is better than that of the biphenyl core since it has more resonance structure and higher radical stability. Three EL devices: ITO/2-TNATA/**HTM 2**/EML/Alq_3/LiF/Al (device IV), ITO/2-TNATA/**HTM 3**/EML/Alq_3/LiF/Al (device V), and ITO/2-TNATA/**HTM 4**/EML/Alq_3/LiF/Al (device VI), were fabricated in order to estimate their suitabilities as a hole transporting material in comparison with the reference device; ITO/2-TNATA/**HTM 1**/EML/Alq_3/LiF/Al (device III)**.** The structures of EL devices are shown in Fig. 4. Fig. 6 shows the luminance and the applied voltage characteristics in the four devices. The luminance of the device IV reached 4,561 cd/m^2 at 6.5V.

Surprisingly, the devices IV-VI with **HTM 2-4** as a hole-transporting material showed a significant enhancement of the luminous efficiency compared to reference device III. The luminous efficiency of the device IV is about 40% higher than that of the device III. The luminous efficiencies of other two devices were also higher than that of the device III. The luminous efficiencies of the device IV-VI with **HTM 2-4** were 8.52, 7.98 and 7.50 cd/A, respectively. Table 2 shows the EL performances of all devices at 6.5V and Fig. 7 shows the current efficiency-applied voltage characteristics.

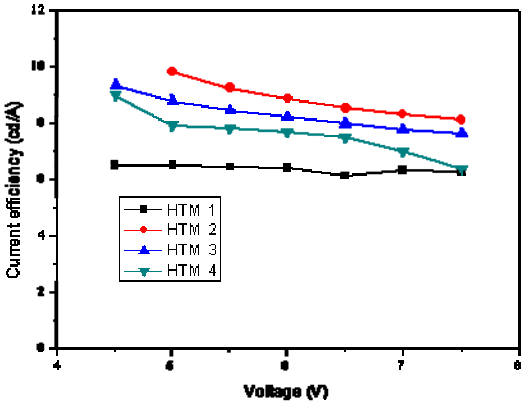

Fig. 7. Current efficiency–applied voltage characteristics of devices III-VI.

Device	Current density (mA/cm^2)	Luminance (cd/m^2)	Current efficiency (cd/A)
Device III	39.01	2383.2	6.11
Device IV	53.54	4561.6	8.52
Device V	46.48	3708.9	7.98
Device VI	53.87	4041.0	7.50

Table 2. EL performance of four devices III-VI at 6.5V

As shown in Table 2, the devices IV-VI using **HTM 2-4** as a hole-transporting material showed remarkable current density and current efficiency performance compared to the reference device III. Fig. 6 shows the devices III needs higher electric power than the devices IV-VI at the same luminance. In other words, it is thought that phenylnaphthydiamine derivatives **HTM 2-4** have superior hole-transporting abilities than biphenyldiamine derivative **HTM 1**. As we mentioned before, these high performances of the devices IV-VI, using phenylnaphthyldiamine derivatives might be attributed to the more efficient hole transportation and higher T_g of those compounds compared to that of biphenyldiamine derivative.

Fig. 8 shows the life-time characteristics of the device IV and the reference device III. The life-time of the device IV is about two times longer than that of the standard device III within the measured current density, indicating more effective recombination at the emitting layer of device IV. These results indicated that phenylnaphthyldiamine derivatives have higher hole-transporting abilities and stabilities toward electric current than that of biphenyldiamine derivative.

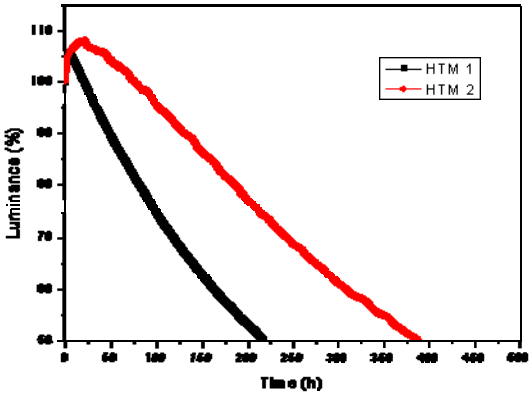

Fig. 8. The life-time characteristics of the two devices at 100mA/cm²; device III (■), device IV (●)

Consequently, hole transporting materials having naphthalene moiety are more stable in radical cation state because of more resonance form and sterically more favored than that of phenyl moiety because of retardation of dimerization reaction. These two factors can contribute to the enhancement of the hole transporting ability resulting in better OLED performance. The device of fluorescent blue OLED using phenylnaphthyldiamines as the hole-transporting layer have much better overall EL performance and longer life-time than the reference device with biphenyldiamine layer.

2.2 Materials for electron transporting

Above mentioned, although OLEDs have shown high brightness and vivid color, long-term stability and image sticking remains a critical issue for practical applications. Device degradation is also largely attributed to the delamination between different layers and the crystallization of organic materials due to electrochemical reaction on interfaces. In general, degradation in OLEDs essentially appears in the form of a decrease in device luminance with time. The decrease in luminance can proceed through three independent and visually distinct modes. These modes are referred as (i) dark-spot degradation, (ii) catastrophic failure, and (iii) intrinsic degradation [23]. These well known degradation mechanism is related with intrinsic material properties as well as device structure.

Recently, it was elucidated that dipole moment of ETM (electron transport material) could be an important factor of initial luminance decrease in OLED. It is well known that luminance decrease at initial phase is a main reason for image sticking. In this chater, we will focus on electron transporting material-dependent life-time pattern and found the relationship between dipole moment of electron transpoting material and initial life-time tendency. it is explained how dipole moment of ETM affected initial luminance decrease in OLED [24-26].

To elucidate a cause of luminance decrease, it has been designed and synthesized a series of ETMs with different value of dipole moment and evaluated the initial life-time of the OLED device using them as ETM.

2.2.1 Dipole moment of electron transporting materials

Dipole moment values for each ETM were calculated by using GAUSSIAN 03 program package. We generated the optimized geometric structure by means of time-dependent density functional theory (TD-DFT) [27],[28] and each dipole moment value was included in the calculation summary. Dipole moments of ETMs were enlisted in Fig. 9 (ADN (Anthracene dinaphthalene) derivatives), Fig. 10 (Phenanthroline derivatives) and there were dipole moment differences among the ETMs according to the arrangement of heteroatom in the molecules. The ETMs were designed in order to minimize the effect of molecular size (Induced dipole-induced dipole interaction or London force) and dipole-dipole interaction is predominant intermolecular force among them.

Structure	Name / Dipole moment (Debye)
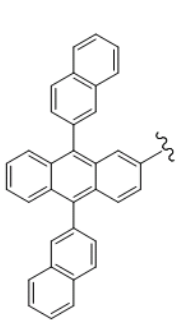 	ET1 3.4774
	ET2 2.9772
	ET3 2.5572
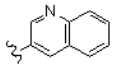	ET4 2.0040

Fig. 9. Molecular structure and calculated dipole moment of ADN series ETMs

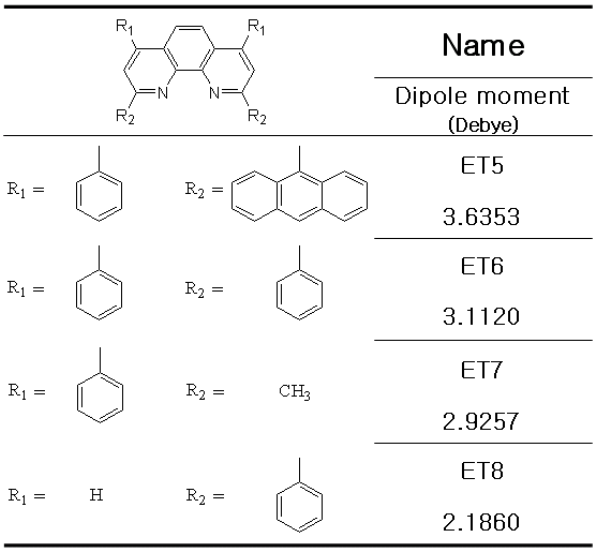

Fig. 10. Molecular structure and calculated dipole moment of Phenanthroline series ETMs

2.2.2 Device fabrication and characteristics

All OLEDs were fabricated on indium tin oxide precoated onto glass substrate. Organic layers were vacuum deposited via thermal evaporation in the high-vacuum chamber. Fig. 11 shows the structure of blue OLED device and its energy diagram. The thickness and materials of each layer are same for fabricated devices except ETMs to eliminate another possible luminance attenuating factor.

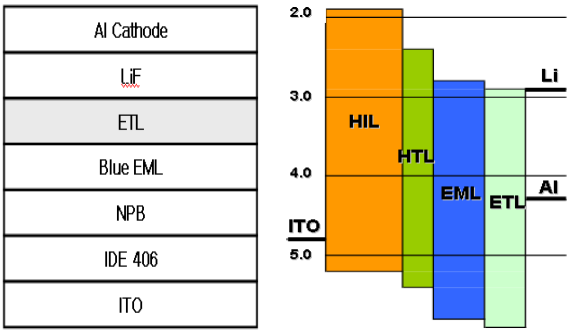

Fig. 11. Blue OLED structure and Energy diagram

The IVL (current density, applied voltage, luminance) characteristics of OLEDs were measured using a Photo Research Inc. PR-650 spectrometer. The operational life-time characteristics were determined from a series of measurements of changes in luminance and drive voltage as function of time under DC driving conditions.

Devices performance properties depended on ETMs and their ability to transport electron [29]. Fig. 12 and Fig. 13 showed I-V and L-Efficiency characteristics of ADN series ETMs, respectively. Regardless of dipole moment differences, device performances depended on the electron transporting ability of the hetero-aromatic rings attached to ADN backbone, and similar property tendency was observed when we applied those hetero-aromatic rings to another framework before. **ET4** (quinoline moiety) gave the best electron transporting performance, but **ET2** (iso-quinoline) showed poor electron transporting ability. In spite of different electronic structures of hetero-aromatic rings, Pyrimidine(**ET1**) and pyridine(**ET3**) moieties exhibited similar properties.

Similar to the results of the ADN series ETMs, it was difficult to explain the result in dipole moment aspect, and device performance characteristics mainly due to the property of phenanthroline stacking. **ET7** and **ET8** are simple structure with minimum appendages and almost flat 3-D structure, so they can be effectively stacked through π-π interaction in deposited layer. On the other hand, relatively bulky side aromatic rings obstruct stacking of phenanthroline moiety. It is well known that π-π stacking among ETMs in deposited layer can enhance electron transporting ability, and that is corresponded with the results of the phenanthroline ETMs [30].

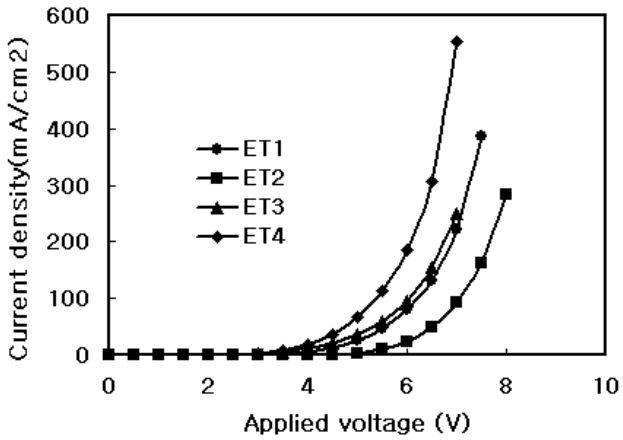

Fig. 12. Voltage-Current curve of ADN series ETMs

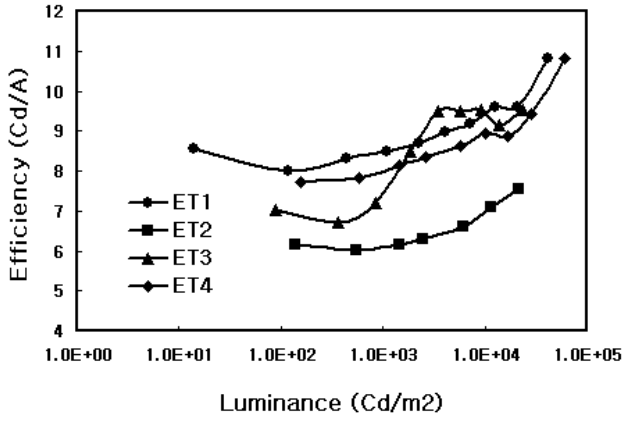

Fig. 13. Luminance-Current efficiency curve of ADN series ETMs

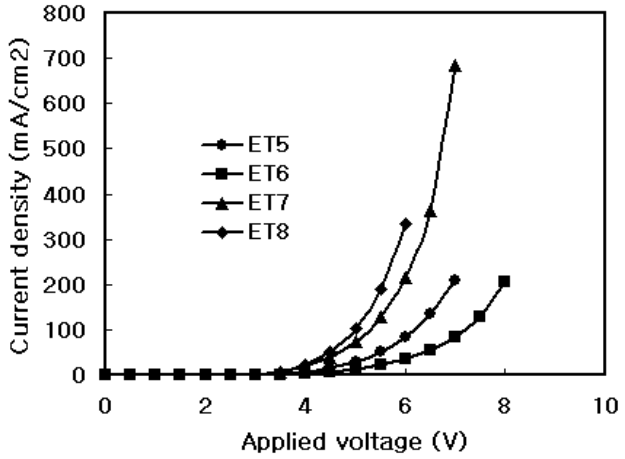

Fig. 14. Voltage-Current curve of Phenanthroline series ETMs

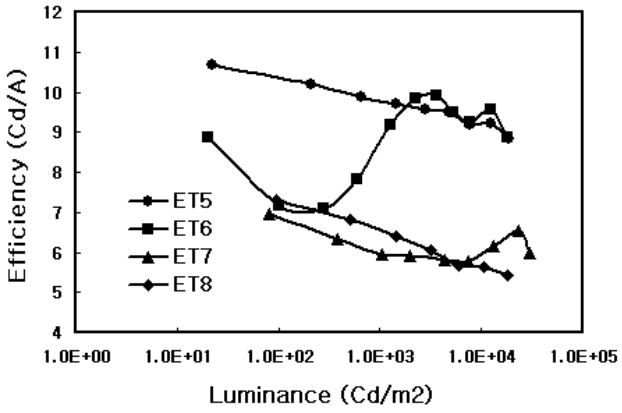

Fig. 15. Luminance-Current efficiency curve of Phenanthroline series ETMs

2.2.3 Analysis of Initial Luminance Decrease

Contrary to the results of performance property, initial phase tendencies of life-time were well corresponded with the dipole moment values. As showed in Fig. 16, the rate of an initial luminance was decreased in the order of **ET1**, **ET2**, **ET3**, and **ET4**, which is contrary to the direction of the dipole moment increase in Fig. 9. **ET1** that can form a robust deposited layer through strong dipole-dipole interactions showed moderate luminance decrease tendency. It can stack regularly in order to form intermolecular network through localized charge distribution in the molecules. It is supposed that an electrically polarized material located under electric field is torqued by an applied electric force and tends to rotate (Fig 17).

When a high electric field is applied, if a material has great dipole moment, phase transformation is difficult to occur in the layer owing to strong intermolecular interactions among deposited molecules (Fig 18a). On the other side, because a low dipole moment material (**ET4**) could not have strong intermolecular force, it cannot stack in compact manner. So it forms less tight layer than materials with strong dipole moment. As depicted in Fig. 18b, deposited molecules rearrange along the electric field or bond strain could be generated in the molecule, and if there is a weak chemical bond, that could be broken when high electric field is applied. In the event, a device composed of small dipole moment ETM showed a steep slope in time-luminance graph at initial phase.

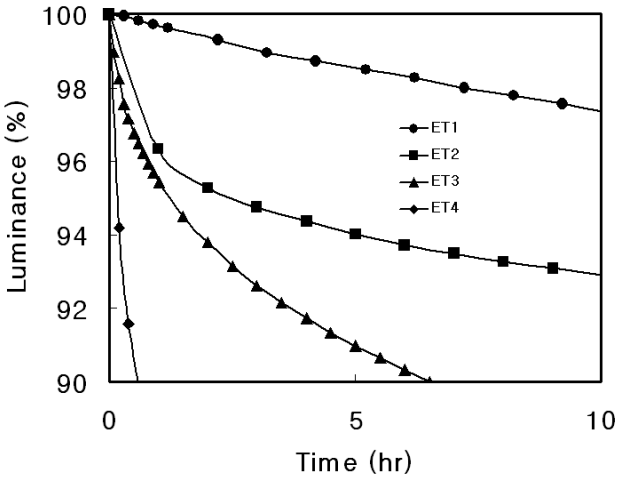

Fig. 16. Initial luminance decrease tendency of devices with ADN series ETMs at 100mA/cm².

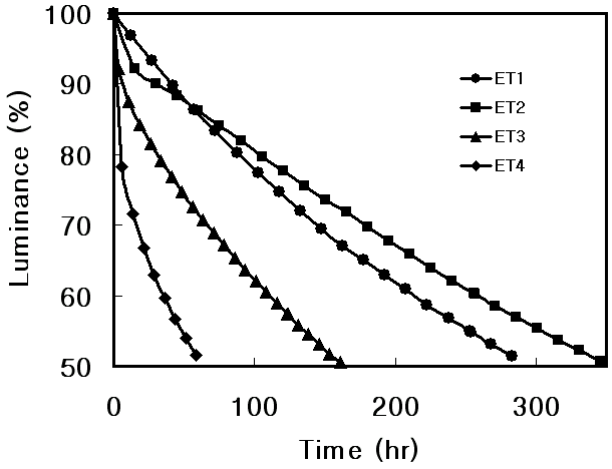

Fig. 16. Life time (half-life) tendency of devices with ADN series ETMs at 100mA/cm²

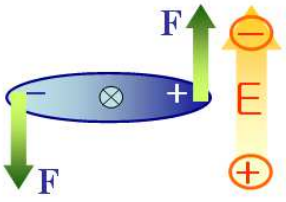

Fig. 17. Behavior of a polarized molecule when electric field is applied

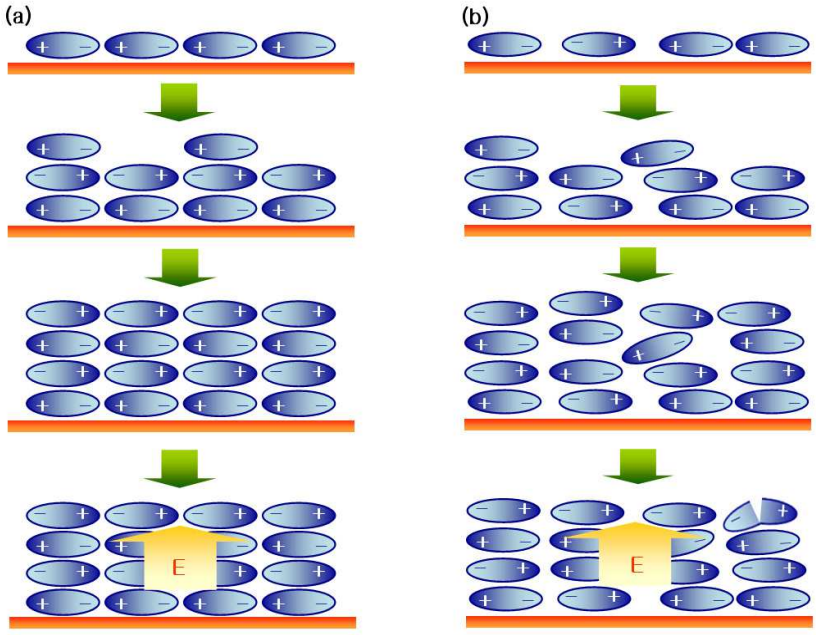

Fig. 18. Schematic descriptions of layer stacking and behavior pattern of polarized molecules under electric field. (a) Material with great dipole moment (b) Material with small dipole moment

Pattern of half-life was similar to that of initial phase, but there must be another factor that could affect life-time. There are some assumed mechanisms for luminance decrease or device degradation [31],[32]. For example, degra- dation of the interface between deposited layers, shift of exciton recombination zone from emitting layer, intrinsically weak chemical bond of used materials and there must be a lot of possible degradation mechanism we could not conceive.

For the test result (Fig. 16), **ET2** showed dramatic luminance decrease in the initial stage, but after initial rearrangement of molecules in the layer, luminance decreased in a moderate manner. On the other hand, luminance decrease rate of **ET1** device was almost constant over all in operation.

Same luminance decrease tendency was observed in phenanthroline series ETMs. Fig. 19 showed the initial luminance of the devices decreased according to the dipole moment order of ETMs, but half-life in Fig. 20 showed a little different degradation order like the case of the ADN series ETMs. **ET6** and **ET8** gave moderate overall life-time graph, and, **ET5** and **ET7** showed Different stacking pattern caused by dipole moment differences could affect density of deposited layer. If the deposited molecules can interact more tightly each other, density of the deposited layer is greater than less tightly interacting one. Actually, density of deposited layer could be influenced by molecular shape and dipole moment. And to avoid ambiguity from structural differences, we measured densities of **ET1** and **ET3** using XRD

[33] because these two materials are spatially same structure except C-H and N. Densities of **ET1** and **ET3** are 1.25 g/cm^3 and 1.21 g/cm^3 respectively, and this result reflects dipole moment differences. Density differences of the deposited layers also provided a clue for elucidating effect of dipole moment on the pattern of luminance decrease at initial phase.

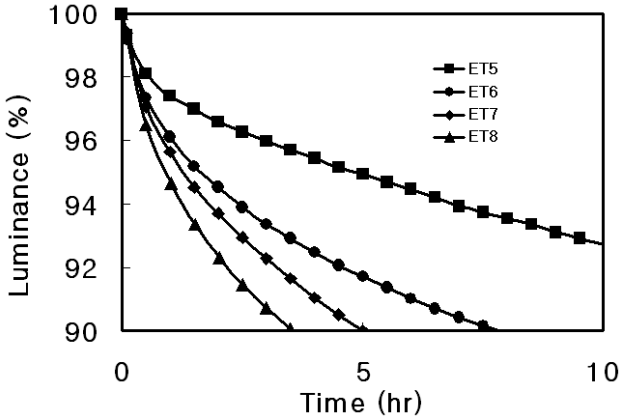

Fig. 19. Initial luminance decrease tendency of devices with Phenanthroline series ETMs at 100mA/cm^2 relatively rapid degradation appearance.

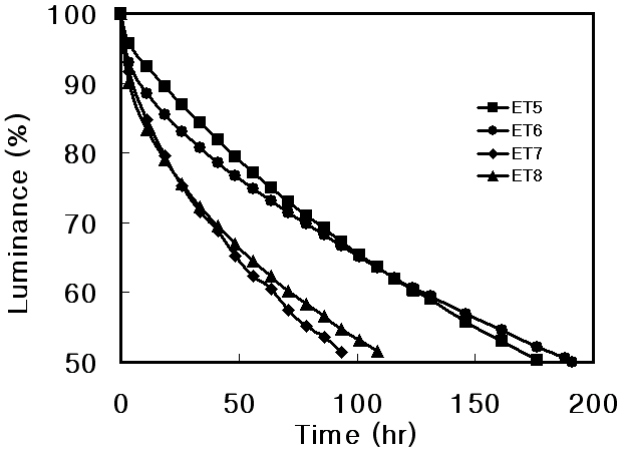

Fig. 20. Life time (half-life) tendency of devices with Phenanthroline series ETMs at 100mA/cm^2

It is concluded that the life-time properties at initial phase were controlled by dipole moment differences of ETMs and great dipole moment materials can enhance initial luminance properties by means of strong dipole-dipole interactions among the molecules. In near future, it is expected to find out a general mechanism of dipole moment effect on life-time.

3. Material issues for new applications of amoled

For future display technologies, there is significant interest in providing display devices with mechanical flexibility and transparency. And also, there are continuous requirements for ultra-thin display and extendable or foldable display without seam line between the two panels. Definitely, it is hardly allowed to manufacture transparent, paper-thin, foldable and flexible displays with the other display technology except for AMOLED.

3.1 Electrode materials for transparent OLED

Since Tang's report on the two-layered organic light emitting diode (OLED), top-emitting organic light emitting diodes (TEOLEDs) with their major advantages of the self-emission of light, wide viewing angle and low power consumption have acquired considerable interest [34-38]. Recently, a number of full-color TEOLEDs have already been introduced into the display market. Especially, OLEDs with transparent cathode are expected to be the next generation displays because of their possible applications for transparent organic light emitting diodes (TOLEDs) which can emit light through both anode and cathode.

Transparent display can be defined as the display across which objects can be seen. Transparency is very attractive feature in the area of display device because it provides both new functional characteristic and plentiful imagination in design. PNS (Private Navigation System) with Augmented Reality technology can come true with the function of transparency in display. Transparency can enlarge its degree of freedom in the conceptual design of PID (Public Information Display) system. It is able to be an important factor which opens up new area of display applications. In addition, Transparency can be secured only with OLED until now on account of its structural simplicity. Because polarizer is not obligatory element in the OLED devices but in the LCD devices, OLED can be a unique display device with its transparency feature.

In most TEOLED, semi-transparent metal such as Mg:Ag is used as a cathode with good electron injection properties. However, resistance and transparence of Mg:Ag cathode is not enough to be applied to the TOLEDs. Recently, many efforts have been made to use indium tin oxide (ITO) and zinc oxide (ZnO) doped with impurities as transparent cathode by sputter deposition method [39-42]. However, the sputtered metal oxide films have some drawbacks on the device stability. It has already reported that the high sputtering power and their high work function led to failures of TOLEDs [43]. While double layer cathode structures of metal/metal have also been investigated, the transmittance of the layer reached at most around 70% which could not be used as the transparent cathode [44,45]. Another researchers tried to developed the ITO films with low work function by introducing a monolayer of strong electron-donor molecules such as tetrakis-(dimethylamino)ethylene, TDAE [46]. However, it is turned out for the efficiency of electron injection to be low.

Recently, Ryu and Baik have already created a TOLED using an indium tin oxide (ITO)/Ag(metal)/ITO (IMI) cathode with low resistance. However, an IMI cathode showed low transmittance due to the low substrateheating through e-beam deposition,2,6,7 and an ITO/Ag/tungsten oxide (WO3) (IAW) for higher transmittance was used in this instance. The Al 20 nm showed a transmittance of 43% and a sheet resistance of 13 ohm. The IMI, WO3 /Ag/WO3, SiO2/Ag/SiO2, and IAW exhibited a transmittance of 27%, 90%, 68%, and 40% at 550 nm respectively. Although the multilayer consisted of a single layer with poor transmita tance, they showed little decrease in transmittance because there is a light

pathway due to multiple reflections. However, it could not be used as a cathode for TOLED due to poor electron injection properties. Therefore, in order to gain the good device characteristics and stability, it is necessary that damage-free cathode material with low work function, low resistance and high transparency is developed.
In spite of many problems as menstioned above, it could be overcomed obstacles by developing highly conducting oxide material without damage to organic layers and by newly designed thermal deposition method. Opimization of device structure can be also made a progress for the transparent cathode structure having electron injection property that were superior to a conventional OLED.
Unlike heat-deposited atoms, sputtered atoms with a high energy could damage the underlying organic layers during the deposition process. To avoid any damage, our cathode films were deposited by the ion beam assisted thermal deposition (IBAD) process using reactive technique. First, we could obtain single-component oxide cathode, indium oxide (InOx) with high work-function by using the thermal process. InOx based films are widely used as transparent cathodes for OLEDs because of their excellent properties of both a high transmittance in the visible region and a low electrical resistivity. In the case of single-component oxide cathode, InOx, although we obtained enough transmittance (Fig. 21(a)) and low electrical resistivity of 20 Ω/, there remains difficulty in using the thin film as a cathode electrode. The difference between LUMO of typical electron transporting layer (ETL) materials, 2.8~3.2eV, and work function of the InOx film, 4.8~5.0eV, is too big to overcome the energy barrier, even if electron injection layer (EIL) such as LiF is used to assist electron injection from the cathode. Therefore, in order to improve electron injection efficiency, new cathode structure with excellent charge injection is required. The electron injection could be improved dramatically without decreasing the transmittance of the InOx cathode structure by using a thin Mg and C60 layers. However, even if our cathode structure enhanced electron injection, it was still important to improve the work function of transparent cathode itself because our device performances were not enough to reach the performance of conventional OLED using cathode of Al/LiF.

3.1.1 Physical properties of new transparent electrode materials

The most suitable cathodes are metals having low work functions ranging from 2.63 to 4.30 eV [47]. In most case, these include Al, Mg, Ca, Ag, Mg:Ag. Especially, Ca has the lowest work function value of 2.63 eV. For improving the work function of transparent cathode, therefore, an InOx electrode doped with Ca was fabricated by the IBAD technique at different deposition rates. The process employed reactive evaporation to grow the InCaOx (ICO) films. The ICO films were deposited by the ion beam assisted thermal evaporation technique using In (wire, 99.99 %) and Ca (3 mm random piece, 99.9%) reactive evaporation at the substrate temperature of 85 ^{o}C. The evaporation of In and Ca is performed steadily at the Ar and O2 gas flow rate of 10 sccm. The time of evaporation recorded, in order to calculate the evaporation rate. The deposition pressure is below 5×10^{-7} torr and typical deposition rates are 0.3 ~ 1.0 □ /sec. The film thickness was measured by an alpha-step system. The optical transmission spectra of the films and the sheet resistances were measured using a UV-VIS spectrophotometer (Perkin Elmer, Lambda 950) and a four-point probe, respectively. The spectral region used in this work was 400-700 nm. The work function was measured using a UV spectrometer (RIKEN KEIKI, AC-2) in the atmospheric

environment. The structure and atomic composition of the thin films were studied by SEM, XRD and X-ray photoelectron spectroscopy (XPS).

The typical transmission spectra as a function of the Ca deposition rate are shown in Fig. 21(a). A high transmittance above 92% in the visible range was obtained in the ICO films deposited on the substrates above approximately 85□. Significantly, it was found that the transmittance in the visible range could be improved in the ICO films deposited on the low-temperature substrates by introducing O_2 gas. The enhancement of the transparency of the ICO film is attributed to the partial oxidation of Ca during the deposition. Furthermore, it is possible that the high energy level of CaO (1.7 eV) which is built up through the reactive IBAD process enhance the injection efficiency of electron.

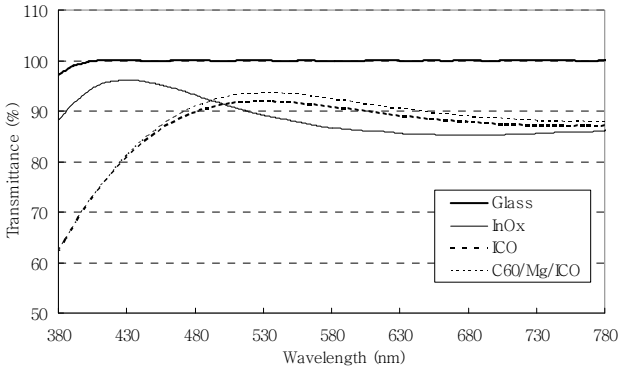

(a)

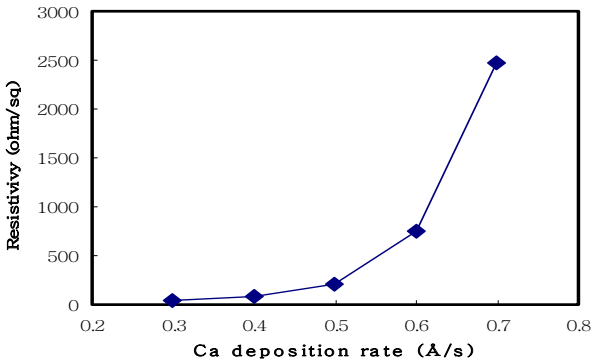

(b)

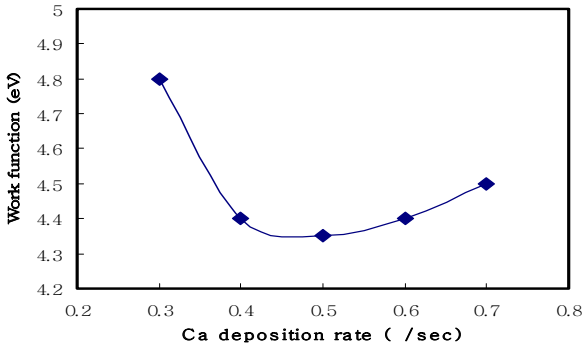

(c)

Fig. 21. (a) Transmittance spectra of ITO and ICO films. (b) work function and (c) resistivity of the ICO film as a function of Ca deposition rate.

The work function and resistivity of the ICO films are shown in Fig. 21(b). In this figure, the measured work function and resistivity of the transparent conducting ITO films prepared by r.f. magnetron sputtering were plotted. The work function of obtained ITO was about 4.9 eV. This value was approximately equal to that measuring other ITO. ICO film had the lowest work function and resistivity between the rate of 0.4 and 0.5 □/sec. The work function of the ICO film was very stable in the ambient atmosphere environment over an extended period of exposure. It can be concluded that the work function of the ICO films, which are possible to use, is in the range from 4.35 to 4.80 eV. Therefore, these films could be selected for use as the cathode. The lowest electrical resistivity value of the film obtained at a Ca deposition rate of 0.1 □/sec while keeping the other deposition parameters. It can be seen that the Ca deposition rate has a strong influence on the conductivity of the films, with the conductivity ranging between 45 and 2469 Ω/ for the films deposited at 0.3 and 0.7 □/sec, respectively. Therefore, the electron injection efficiency is primarily due to Ca metal having a low work function (2.9 to 3 eV), while the Ca metal increases the lateral electrical conductance of the ICO film. Consequently, ICO film which was deposited at 0.4 □/sec was choose owing to the appropriate value of work function and resistivity as a cathode for TOLEDs.

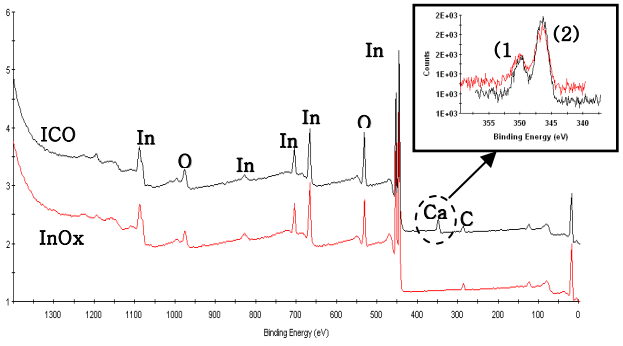

(a)

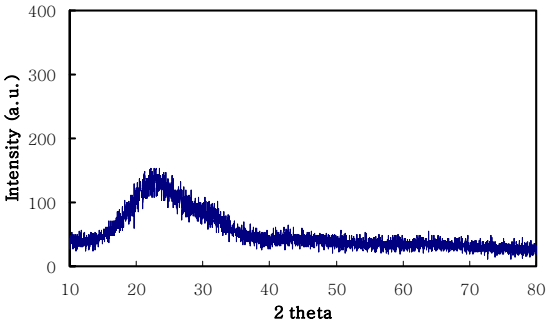

(b)

Fig. 22. (a) XPS wide scan and (b) XRD diffraction spectra of the ICO film.

The XPS wide scan spectra in Fig. 22(a) is from a typical InOx and ICO film on a Si wafer. In addition to the In and O features, a Ca $2_{P3/2}$ peak at 346 eV is clearly observed. The inset figure shows the narrow scans of the spectra around (1) Ca $2_{P1/2}$ and (2) Ca $2_{P3/2}$. The XPS data showed that only the ICO films have definitive Ca peaks for $2_{P3/2}$ whose estimated concentration was approximately 3 %. The surface chemistry and morphology are known to have dramatic impact on charge transport across the organic-TCO interface. The XRD pattern also showed no diffraction peaks, so that the ICO film should be amorphous with no visible pores or larger interface defects, as well as having a smoother surface (Fig. 22(b)). The surface morphology also has a strong influence on the optical and electrical properties of the films, since the textured surfaces lead to the enhancement of the light collected. Fig. 23 shows the SEM images of (a) the commercial ITO and (b) ICO film, in which the ICO film is observed to exhibit a more smooth and homogeneous surface, compared with the ITO film. In the case of commercial ITO, crystallization leads to the formation of a polycrystalline structure. The ICO films are amorphous with low surface roughness (RMS, Ra=1.1 nm), since they are fabricated using a slower deposition rate or lower temperature.

We investigated for IBAD process to induce damage to organic layers. In general, leakage current is observed during reverse sweep, if the organic bond in ETL is broken or damaged by energetic particles during the deposition. While typical sputtered ITO film gave a serious damage to organic layer, as is shown in Fig. 24, there is no leakage current in the transparent conducting film, keeping the current below 10^{-5} mA in the reverse bias region in J-V curve.

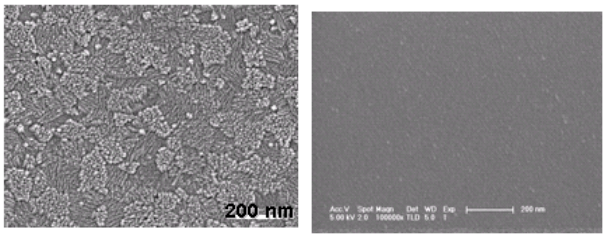

(a) (b)

Fig. 23. SEM (Scanning Electron Microscope) images of (a) Commercial ITO and (b) ICO film fabricated by the ion beam assisted thermal evaporation.

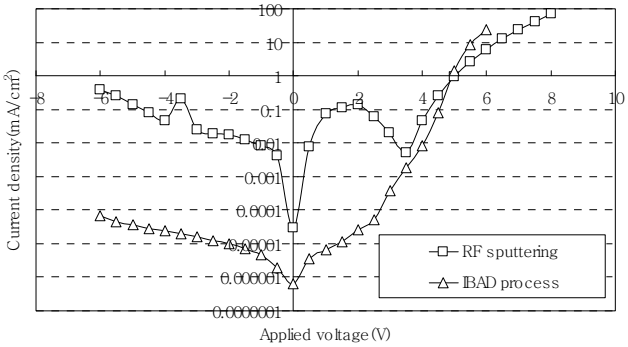

Fig. 24. Current density-voltage curves of ITO-deposited OLED with RF sputtering and ICO-deposited with IBAD thermal process at 85°C.

3.1.2 Device fabrication and characteristics

To study the cathode dependence to the device performance, various device structures were manufactured. The device configuration of the TEOLEDs was Ag (100 nm)/ITO (10 nm)/*N,N'*-diphenyl-*N,N'*-bis-[4-(phenyl-m-tolyl-amino)-phenyl]-biphenyl-4,4'-diamine (DNTPD, 60 nm)/*N*, *N'*-di(1-naphthyl)-*N,N'*-diphenylbenzidine (NPB, 30 nm)/distyryl anthracene(DSA):tetra(*t*-butyl)perylene (30 nm, 100:5)/bis(10-hydroxybenzo[h]quinolinato)beryllium (Bebq2, 20 nm)/cathode. A basic electrode structure of transparent cathode (100 nm)/Mg (7 nm)/LiF (1 nm)/C60 (2 nm) was used in the TEOLEDs after optimizing the thickness of Mg and C60 layers (Fig. 25).

The devices were fabricated on glass substrates precoated with a high-work-function anode such as indium–tin–oxide. The ITO substrates was cleaned in deionized water, and given an UV-ozone treatment prior to use. In the case of an anode with Ag reflector, EL was observed through a transparent ICO cathode. The active area of our devices was 4 mm^2. Prior to use, all organic materials were purified by vacuum train sublimation. Deposition of the organic materials was carried out in a high vacuum system (Sunic) by thermal evaporation from resistively heated alumina crucible. The base pressure in the chamber ranged between $4x10^{-7}$ and $1x10^{-6}$ mbar. Typical deposition rates were 1 Å/s. The evaporation chamber was attached directly to a nitrogen glove-box system, which allowed devices to be fabricated, characterized, and encapsulated under inert conditions. *I–V* and luminance–voltage characteristics were measured with a Kiethley 237 programmable electrometer and Photo research PR650 spectroradiometer.

As shown in Fig. 26(a), the current density-voltage properties of the devices having the IBAD-processed InOx cathodes were correlated with the electrode structure. The Mg and C60 thin layer was incorporated to ensure efficient electron injection. It is believed that the work function of Mg, 3.6 eV, can decrease the energy barrier between indium oxide and ETL material. Feng et al. have already found that metal/LiF /C60 interface exhibits ohmic type junction characteristics whereas metal/C60 interface exhibits rectifying Schottky-type junction characteristics [48]. They described the role of C60 in the cathode structure as like the followings. First, $F^-(-Li^+)$ anions introduce an *n*-type doping zone near the interface. The *n*-type doping was found by x-ray photoelectron spectroscopy analysis of LiF-doped C60

films. Second, a recent calculation suggests that LiF-C60 interaction leads a reduced energy gap and thus lead to a metallic interface.

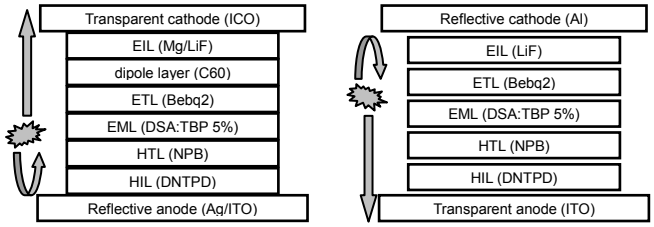

(a) (b)

Fig. 25. Schematic device structures of (a) TEOLED with transparent cathode and (b) conventional OLED.

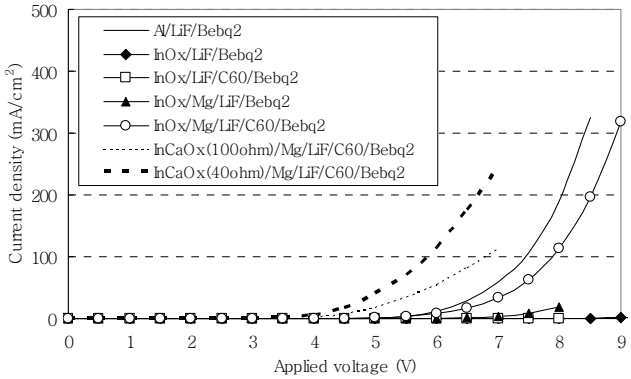

(a)

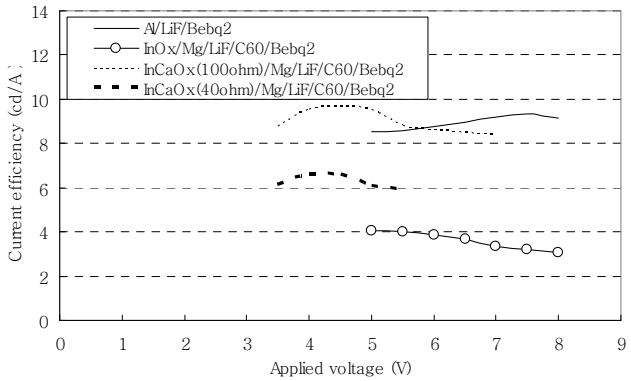

(b)

Fig. 26. The performances of OLEDs as the various cathode structures; (a) current density-voltage and (b) current efficiency-voltage.

In order to compare the characteristics of ICO with those of InOx, we also investigated the performance of devices having ICO. The resistance of ICO, 30 Ω/□, is slightly higher than that of InOx, 20 Ω/□. However, operational voltage of device having ICO is lower than that of InOx at the same current density. This indicated that the insertion of Ca metal between ICO and Mg is effective reducing the drive voltages and improving device efficiency. Moreover, as shown in the Fig. 26(a), ICO which is reduced the resistance of 30 Ω/□ presented lower operational voltage than ICO with the resistance of 100 Ω/□. These results clearly demonstrate that J-V performance is better as the resistance is lower in the case of same electron injection efficiency. Consequently, transparent cathode should have low resistance and low work function for good J-V performance of OLED device.

In spite of good J-V performance, however, we can not always expect for the OLED device with high current density to present high current efficiency. Even though a device which have so much electron carrier or hole carrier shows high current density, the recombination zone of the device could not be formed in emitting layer. Fig 26(b) shows the current efficiency of the devices having the different transparent cathode. The highest current efficiency value of 10 cd/A was obtained from the device having the 100 ohm ICO. The hole injection efficiency is very similar to the every devices because of the same structure of ITO/HIL/HTL/EML. From this assumption, it can be thought that the current efficiency of OLED having ICO is greatly affected by electron injection efficiency between ETL and cathode structure. Therefore, it can be also supposed that the charge balance of both device having Al/LiF and 100 ohm ICO is superior to other cathode structure.

For the better J-V characteristics and the decrease of IR drop, it is needed to acquire lower resistance of cathode. So we fabricated the gradient Ca-doped ICO which was not doped with Ca to the whole range of InOx, but doped with Ca to the only shallow interface (about 50 Å) between InOx and Mg layer. We could improve the resistance of the newly designed cathode structure with this gradient Ca-doped ICO (gradient type ICO).

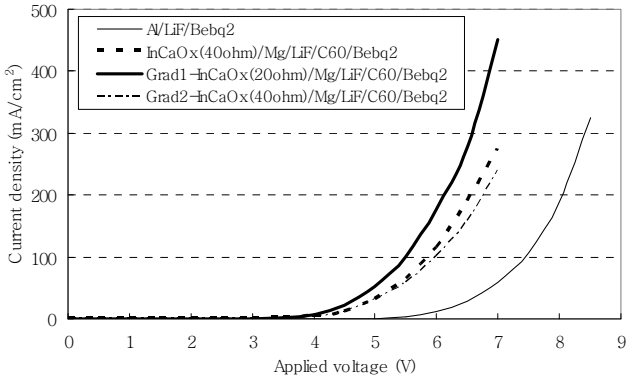

(a)

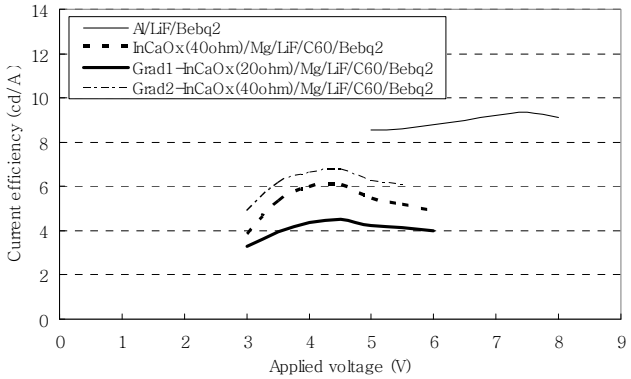

(b)

Fig. 27. The performances of OLEDs with ICO and gradient doped ICO; (a) current density-voltage and (b) current efficiency-voltage.

Fig 27 shows the J-V performance of the device having gradient type ICO. As like our initial intention to the correlation between the resistance of ICO and J-V characteristics of device, the lower resistance of ICO lead to the lower applied voltage at the same current density. Simultaneously, in the case of current efficiency, the similar J-V characteristics lead to the similar current efficiency. This result is very concurrent with the former result of Fig 26. From the same value of resistance and J-V curve, it can be thought that the electron injection efficiency is very similar for the both cathode of ICO and gradient type ICO with similar resistance. Furthermore, the similar J-V current and resistance derived the similar current efficiency from each devices. Then it is also supposed that J-V and current efficiency is determined by electron injection in the case of the similar hole injection properties and electron injection is defined by the energy barrier of ICO-Mg interface. Hereafter, in order to acquire the better properties of OLED device with ICO, it is needed to improve the mobility and injection property of HIL and HTL for controlling the recombination zone and enhancing the J-V characteristics and current efficiency.
In conclusion, new transparent and conductive ICO films were fabricated by ion beam assisted thermal evaporation. From the results of this study, it is possible to conclude that the use of a dopant leads to significant changes in the optical and electrical properties of the ICO films. In fact, it was found that the electrical conductivity (30 Ω/□) and work function (4.35 eV) of the films thickness of 1000 Å can be controlled by adjusting the Ca deposition rate, thereby allowing us to attain films with desirable properties. Optical transmission higher than 92% was measured in the visible region. In addition, new top-emitting device structure with good device efficiency was proposed by using new cathode structure and transparent cathode materials. These films will be good candidates for transparent cathodes in TOLEDs.

3.2 Encapsulation materials for foldable and flexible OLED

Another unique displays using AMOLED are paper-thin, foldable and flexible displays. A number of technologies are developing towards flexible and thin displays that can be

flapping, like paper (Fig. 28). In these cases, encapsulation technology is most important among various AMOLED technologies. For general AMOLED, edge sealing with the frit which is used for small-sized AMOLED has serious problems such as mechanical strength under external stress. In order to surmount those fatal flaws, new techniques such as filling the gap between two glasses are currently under development. Organic materials are susceptible to water, oxygen and other environmental elements present in ambient conditions. Furthermore, electrode metals deposited on the light-emitting layer are prone to oxidation resulting from exposure to water and oxygen, etc. While commercialized powder-type desiccants have been used for the encapsulation of bottom-emitting OLEDs, these desiccants could not be applied to top-emitting AMOLEDs because they blocked the emitted light due to their opaqueness. So, the transparent film desiccants were used by mixing solutions dispersed with calcium oxide powders and ultraviolet-curable resins. As the solid content in the solutions increased from 15 wt.% to 30 wt.%, the average particle size increased from 107 nm to 240 nm, whereas the transmittance of the films decreased from 98 % to 80 % in the visible range. The devices encapsulated with the transparent film desiccants which contained 20 wt.% CaO exhibited no dark spots and 97 % of the initial luminance, even after being stored for over 500 hrs at 70 ^{o}C and 90 % R.H. Also, the operational lifetime of these devices was 1850 hr, 10 times longer than that of device without desiccant. These results confirmed that the transparent film desiccants which absorbed the moisture that penetrated into the devices could be applied to the encapsulation of top-emitting AMOLEDs. However, Paper-thin, foldable, flexible even flapping AMOLEDs can't be easily made by normal encapsulation method which seals with hard encapsulation glass and desiccants. Instead of that, thin film encapsulation technology should be employed that protects the organic device but leaves it thin and flexible. Thin film encapsulation is very powerful solution for obtaining unique characteristics of AMOLED [49]. Instead of using upper encapsulation glass, TFE employs layer-by-layer deposition of thick films with compensating diffusion barrier properties. The biggest merit of TFE is that it enables single glass display, which makes extremely slim and flexible panels possible. The challenges for TFE include material optimization, minimization of stacking layers, and applicability for large size mother glasses. Figure 29 shows SEM image of thin film encapsulated OLED which consist of inorganic and organic alternative layers.

Fig. 28. 6.5" flexible AMOLED display by Samsung.ufigureLOGICAL ISSUES FOR SMALL-SIZED MOBILE OLEDD

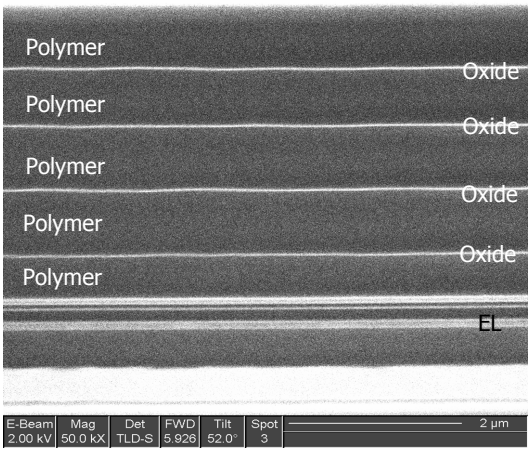

Fig. 29. SEM image of thin film encapsulated AMOLED.

4. Summary

In this article, we presented the organic material issues for common AMOLED. It was also reviewed that unique materials of AMOLED could create the new applications such as paper-thin, foldable, bendable and transparent displays. Although there remain some problems unsolved, we are convinced that AMOLED should be the leader of information display in the near future.

5. References

Y. Shirota, J. Mater. Chem. 10, 1 (2000).
T. Fuhrmann, J. Salbeck, Advances in Photochemistry (eds., D. C. Neckers, D. H. Volman, G. von Bünau), vol. 27, Wiley, New York (2002).
U. Mitschke, P. Bauerle, J. Mater. Chem. 10, 1471 (2000).
J. Kido, Bull. Electrochem. 10, 1 (1994).
S. Tokito, Y. Taga, Appl. Phys. Lett. 66, 673 (1995)
P. F. Smith, P. Gerroir, S. Xie, A. AM. Hor, Z. Popovic, M. L. Hair, Langmuir 14, 5946 (1998)
K. Naito, A. Miura, J. Phys. Chem. 97 (1993) 6240.
S. Tokito, H. Tanaka, K. Noda, A. Okada, Y. Taga, Appl. Phys. Lett. 70, 1929 (1997).
B.E. Konne, D.E. Loy, M.E. Thompson, Chem. Mater. 10, 2235 (1998).
F. Steuber, J. Staudigel, M. St¨ossel, J. Simmerer, A. Winnacker, H. Spreitzer, F. Weiss¨ortel, J. Salbe´ck, Adv. Mater. 12, 130 (2000).
P. Strohriegl, J.V. Grazulevicius, Adv. Mater. 14 (2002) 1439.
L. S. Hung and C. H. Chen, Mater. Sci. Eng. R39, 143 (2002).
P. Strohriegl and J. V. Grazulevicius, Adv. Mater. 14, 1439 (2002).
B. E. Konne, D. E. Loy and M. E. Thompson, Chem. Mater. 10, 2235 (1998).
M. Thelakkat and H. Schmidt, Adv. Mater. 10, 219 (1998).
K. Katsuma and Y. Shirota, Adv. Mater. 10, 223 (1998).

I. Y. Wu, J. T. Lin, Y. T. Tao, E. Balasubramaniam, Y. Z. Su and C. W. Ko, Chem. Mater. 13, 2626 (2001).
C. W. Ko and T. Tao, Synth. Met. 126, 37 (2002).
K. T. Wong, Z. J. Wang, Y. Y. Chien and C. L. Wang, Org. Lett. 3, 2285 (2001).
D. E. Loy, B. E. Konne and M. E. Thompson, Adv. Funct. Mater. 12, 245 (2002).
Y. K. Kim and S. H. Hwang, Chem. Lett. 35, 120 (2006).
Y. K. Kim and S. H. Hwang, Synth. Met. 156, 1028 (2006).
H.Aziz, Z.D. Popovic, Chem. Mater., 16, 4522 (2004).
P. M. Borsenberger, J. J. Fitzgerald J. Phys. Chem., 97(18), 4815 (1993).
R. H. Young, T. M. Kung, J. A. Sinicropi, N. G. Rule, J. J. Fitzgerald, J. E. Eilers, C. H. Chen, N. W. Boaz J. Phys. Chem., 100, 17923 (1996).
(a) K. L. Tong, S. K. So, H. F. Ng, L. M. Leung, M. Y. Yeung, C. F. Lo Syn. Met., 147, 199 (2004), (b) H. Bässler Phys. Status Solidi B, 175, 15 (1993) (c) A. Dieckmann, H. Bässler, P. M. Borsenberger J. Chem. Phys., 99, 8136 (1993) (d) R. H. Young Philos. Mag. B, 72, 435 (1995).
DFT calculation method was B3LYP, basis set was 6-31G (d) and charge calculation option was NBO (natural bonding orbital).
E. S. Replogle, G. W. Trucks, S. W. Staley J. Phys. Chem., 95(18), 6908 (1991).
(a) G. He et al ., Proc. SPIE, Vol. 5519, 42 (2004), (b) B. W. E-Andrade et al., Appl. Phys. Lett., 83(19), 3858 (2003), (c) R. H. Friend, R. W. Gymer, A. B. Holmes, J. H. Burroughes, R. N. Marks, C. Taliani, D. D. C Bradley, D. A. Cos Santos, J. L. Bredas, M Logdlund and W. R. Salneck, Nature, 397, 121 (1999).
A. P. Kulkarni, C. J. Tonzola, A. Babel, S. A. Jenekhe, Chem. Mater., 16, 4558 (2004).
J. R. Gong, L. J. Wan, S. B. Lei, C. L. Bai J. Phys.
Chem. B, 109, 1675 (2005).
C. C. Tong, K. C. Hwang J. Phys. Chem. C, 111, 3490 (2007).
Density of 1000Å organic deposited layer was measured by reflectivity simulation using XRD in AE center, Samsung Advanced Institute of Technology.
C. W. Tang, S. A. VanSlyke, Appl. Phys. Lett. 51, 913 (1987).
C. W. Tang, S. A. VanSlyke, C. H. Chen, Appl. Phys. Lett. 65, 3610 (1989).
L. S. Hung, C. W. Tang, M. G. Mason, Appl. Phys. Lett. 70, 152 (1997).
G. E. Jabbour, Y. Kawabe, S. E. Shaheen, J. F. Wang, M. M. Morrel, B. Kippelen, N. Peyghambarian, Appl. Phys. Lett. 71, 176 (1997).
Y. W. Ko, C. H. Chung, J. H. Lee, Y. H. Kim, C. Y. Son, B. C. Kim, C. S. Hwang, Y. H. Song, J. Lim, Y. J. Ahn, G. W. Kang, N. Lee, C. Lee, Thin Solid Films, 46, 246 (2003).
T. C. Gorjanc, D. Leong, C. Py, D. Roth, Thin Solid Film, 413, 181 (2002).
M. Ohyama, H. Kozuka, T. Yoko, Thin Solid Films, 306, 78 (1997).
R. Martins, P. Barquinha, I. Ferreira, L. Pereira, G. Goncalves, E. Fortunato, J. Appl. Phys. 101, 044505 (2007).
T. Yamada, A. Miyake, S. Kishimoto, H. Makino, N. Naoki, T. Yamamoto, Appl. Phys. Lett.
G. Gu, V. Bulovic, P. E. Burrows, S. R. Forrest, M. E. Thomson, Appl. Phys. Lett. 68, 2606 (1996).
R. B. Pode, C. J. Lee, D. G. Moon, J. I. Han, Appl. Phys. Lett. 84, 4614 (2004).
R. B. Pode, C. J. Lee, D. G. Moon, J. I. Han, Appl. Phys. Lett. 89, 123501 (2006).
W. Osikowicz, X. Crispin, C. Tengstedt, L. Lindell, T. Kugler, W.R. Salaneck, Appl. Phys. Lett. 85, 1616 (2004).

K. S. Yook, S. O. Jeon, C. W. Joo, J. Y. Lee, Appl. Phys. Lett. 93, 013301 (2008).
X. D. Feng, C. J. Huang, V. Lui, R. S. Khangura, Z. H. Lu, Appl. Phys. Lett. 86, 1 (2005).
A. B. Chwang, M. A. Rothman, S. Y. Mao, R. H. Hewitt, M. S. Weaver, J. A. Silvernail, K Rajan, M. Hack, J. J. Brown, X. Chu, L. Moro, T. Krajewski, and N. Rutherford, Symposium Digest Tech Papers, 34, 868-871 (2003).

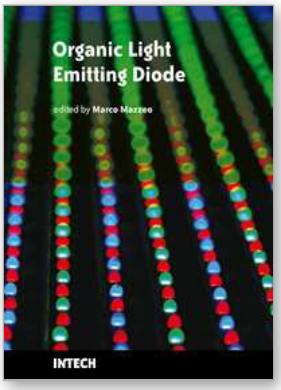

Organic Light Emitting Diode
Edited by Marco Mazzeo

ISBN 978-953-307-140-4
Hard cover, 224 pages
Publisher Sciyo
Published online 18, August, 2010
Published in print edition August, 2010

Organic light emitting diodes (OLEDs) have attracted enormous attention in the recent years because of their potential for flat panel displays and solid state lighting. This potential lies in the amazing flexibility offered by the synthesis of new organic compounds and by low-cost fabrication techniques, making these devices very promising for the market. The idea that flexible devices will replace standard objects such as television screens and lighting sources opens, indeed, a new scenario, where the research is very exciting and multidisciplinary. The aim of the present book is to give a comprehensive and up-to-date collection of contributions from leading experts in OLEDs. The subjects cover fields ranging from molecular and nanomaterials, used to increase the efficiency of the devices, to new technological perspectives in the realization of structures for high contrast organic displays and low-cost organic white light sources. The volume therefore presents a wide survey on the status and relevant trends in OLEDs research, thus being of interest to anyone active in this field. In addition, the present volume could also be used as a state-of-the-art introduction for young scientists.

InTech Europe
University Campus STeP Ri
Slavka Krautzeka 83/A
51000 Rijeka, Croatia
Phone: +385 (51) 770 447
Fax: +385 (51) 686 166
www.intechopen.com

InTech China
Unit 405, Office Block, Hotel Equatorial Shanghai
No.65, Yan An Road (West), Shanghai, 200040, China
中国上海市延安西路65号上海国际贵都大饭店办公楼405单元
Phone: +86-21-62489820
Fax: +86-21-62489821